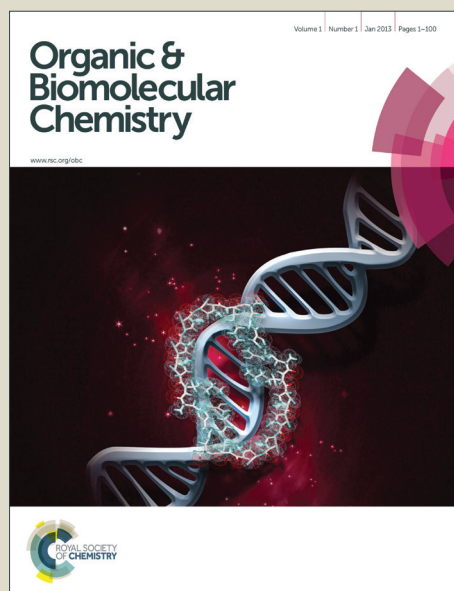


Organic & Biomolecular Chemistry

Accepted Manuscript

This article can be cited before page numbers have been issued, to do this please use: S. J. Glynn, K. J. Gaffney, M. A. Sainz, S. G. Louie and N. A. Petasis, *Org. Biomol. Chem.*, 2015, DOI:



This is an *Accepted Manuscript*, which has been through the Royal Society of Chemistry peer review process and has been accepted for publication.

Accepted Manuscripts are published online shortly after acceptance, before technical editing, formatting and proof reading. Using this free service, authors can make their results available to the community, in citable form, before we publish the edited article. We will replace this *Accepted Manuscript* with the edited and formatted *Advance Article* as soon as it is available.

You can find more information about *Accepted Manuscripts* in the [Information for Authors](#).

Please note that technical editing may introduce minor changes to the text and/or graphics, which may alter content. The journal's standard [Terms & Conditions](#) and the [Ethical guidelines](#) still apply. In no event shall the Royal Society of Chemistry be held responsible for any errors or omissions in this *Accepted Manuscript* or any consequences arising from the use of any information it contains.

Organic & Biomolecular Chemistry

PAPER

Molecular characterization of the boron adducts of the proteasome inhibitor Bortezomib with epigallocatechin-3-gallate and related polyphenols

Stephen J. Glynn,^{a,b} Kevin J. Gaffney,^{a,b,c} Marcos A. Sainz,^{a,b} Stan G. Louie,^c and Nicos A. Petasis^{*a,c,d}

Received
Accepted

DOI: 10.1039/x0xx00000x

www.rsc.org/

The green tea polyphenol epigallocatechin-3-gallate (EGCG) was reported to effectively antagonize the ability of Bortezomib to induce apoptosis in cancer cells. This interaction was attributed to the formation of a covalent adduct between a phenolic moiety of EGCG with the boronic acid group of Bortezomib. However, the structural details of this boron adduct and the molecular factors that contribute to its formation and its ability to inhibit Bortezomib's activity remain unclear. This paper describes the use of NMR spectroscopy and cell assays to characterize the structures and properties of the boron adducts of EGCG and related polyphenols. The observed boron adducts included both boronate and borate derivatives, and their structural characteristics were correlated with cell-based evaluation of the ability of EGCG and other phenols to antagonize the anticancer activity of Bortezomib. The enhanced stability of the BZM/EGCG adduct was attributed to electronic and steric reasons, and a newly identified intramolecular interaction of the boron atom of BZM with the adjacent amide bond. The reported approach provides a useful method for determining the potential ability of polyphenols to form undesired adducts with boron-based drugs and interfere with their actions.

Introduction

The proteasome inhibitor Bortezomib (BZM), also known as PS-341 and now marketed as VelcadeTM (**1**, Fig. 1), is approved for the treatment of multiple myeloma and mantle cell lymphoma.^{1–6} A novel structural feature of BZM is its boronic acid group, which forms reversibly a borate adduct with threonine at the chymotrypsin-like active site of the 26S proteasome, serving as a transition state mimic. Despite extensive efforts in drug discovery aimed at the development of boron compounds,^{7–13} BZM still remains the only approved boron-containing drug. However, in recent years, a growing number of boron-based therapeutics^{8–13} are being investigated

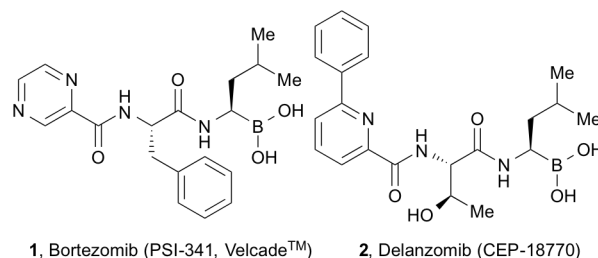


Fig. 1 Structures of boron-based proteasome inhibitors.

in clinical trials, including the new proteasome inhibitor Delanzomib (CEP-18770)^{14–16} (**2**, Fig. 1).

The discovery^{1,2} and clinical development^{4–6} of BZM as an effective therapeutic agent demonstrated for the first time that the selective inhibition of the 26S proteasome¹⁷ is a viable approach for the treatment of cancer.^{3,18–23} Cellular proteasome is a key enzymatic complex in all cells that degrades and recycles targeted and misfolded intracellular proteins. As a key component of the ubiquitin proteasome pathway (UPP) and the

^aDepartment of Chemistry and Loker Hydrocarbon Research Institute, University of Southern California, Los Angeles, California 90089, USA. E-mail: petasis@usc.edu

^bContributed equally to this work as co-first authors

^cSchool of Pharmacy, University of Southern California, Los Angeles, California 90089

^dNorris Comprehensive Cancer Center, Keck School of Medicine, University of Southern California, Los Angeles, California 90089

Electronic Supplementary Information (ESI) available: Other experimental data. See DOI: 10.1039/b000000x/

ARTICLE

unfolded protein response (UPR), the proteasome plays a critical role in cell division and cell survival. Selective and temporary inhibition of the 26S proteasome by BZM or other proteasome inhibitors results in a selective apoptotic effect in cancer cells, which occurs via several mechanisms.²⁴ By blocking the degradation of I κ B, proteasome inhibition partially prevents the activation of the transcription factor NF- κ B, and results in cell cycle arrest and inhibition of cell growth.^{3, 18–23} It also leads to the accumulation of ubiquitinated unfolded or misfolded proteins resulting in the induction of endoplasmic reticulum stress (ER stress).^{25,26} Based on its novel mechanisms of action, BZM has been shown to be effective as a single agent and in combination therapies.^{4, 6, 27}

As part of our efforts towards the development of novel proapoptotic agents for the treatment of various types of cancer, including multiple myeloma,²⁸ lung cancer,²⁹ lymphoma,³⁰ glioblastoma,^{31, 32} and breast cancer,^{33–35} we identified certain molecules that selectively induce apoptosis in cancer cells by increasing ER stress.^{31, 36–42} These ER-stress-aggravating agents (ERSA) are novel anticancer therapeutics and are also effective in certain combinations with other therapies.^{43, 44} In this context, we have investigated the combination of such molecules with BZM.³¹ We have shown that BZM promotes enhanced killing of glioblastoma cells when used in combination with the COX-2 inhibitor Celecoxib, as well as 2,5-dimethyl-celecoxib (DMC) a structural analog that does not inhibit COX-2.³¹ This increased anticancer activity was attributed to a modest increase in ER stress, evidenced by elevated levels of key ER stress markers, such as the chaperone protein GRP78 and the pro-apoptotic transcription factor CHOP. Although cancer cells are able to survive under a hostile microenvironment by adapting to chronic elevated ER stress conditions, even a modest additional ER stress aggravation is not tolerated, triggering cellular apoptosis.

These interesting findings prompted us to investigate the combination of BZM with (-)-epigallocatechin-3-gallate, abbreviated as EGCG (3), the most bioactive polyphenol component of green tea, a commonly used dietary supplement (Fig. 2). Extracts from green tea have attracted great interest from the scientific and alternative medicine communities,⁴⁵ and its chemopreventive⁴⁶ and epigenetic^{47, 48} properties have been shown in multiple animal models of cancer.^{49–51}

Dietary polyphenols^{52, 53} (Fig. 2) are present in large quantities in many common plant-based food components (e.g. green tea, apples, grapes, wine, cocoa, etc.) and recent research has pointed to their potential utility in the prevention of cancer, cardiovascular diseases, osteoporosis, neurodegenerative diseases and diabetes. For example, the bioactivity of (-)-epicatechin (6, EC), and resveratrol (7, RSV),⁵⁴ which are key components of dark cocoa^{54, 55} and red wine⁵⁴ respectively, have received increased interest for their chemopreventive properties. These polyphenols have shown several mechanisms of action as anticancer agents, including regulation of oxidative stress as well and inhibition of cell proliferation.⁵⁵ Also, procyanidin B2 (8), a common component of apples and grapes

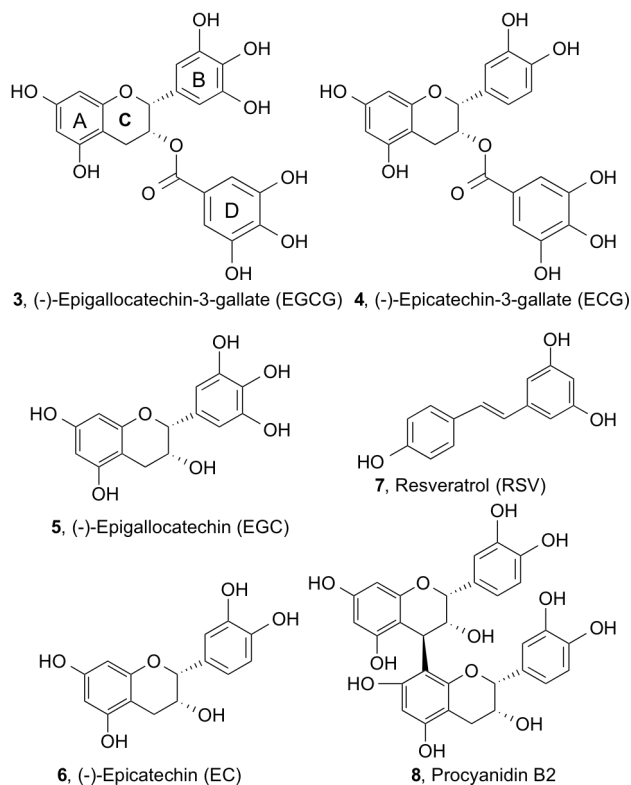


Fig. 2 Structures of EGCG and other dietary polyphenols.

and a dimer of (-)-epicatechin (6, EC), was shown to block the activity of NF- κ B, by preventing its binding to DNA.⁵⁶

The therapeutic effects of green tea have been primarily attributed to its component catechins (Fig. 2), namely (-)-epigallocatechin-3-gallate (3, EGCG), (-)-epicatechin gallate (4, ECG) (-)-epigallocatechin (5, EGC), and (-)-epicatechin (6, EC). These polyphenols were shown to interact with a number of biological pathways including GRP78 a key chaperone protein involved in ER stress.³⁹ Interestingly, it was also reported that EGCG and structural analogs inhibit the proteasome, while their acetylated or methylated derivatives do not show such activity.^{57–65}

In order to examine the potential for synergistic effects of BZM with green tea components, we have investigated the combination of EGCG and related polyphenols with BZM for targeting multiple myeloma and glioblastoma.³⁹ Given the presence of the boronic acid group in BZM, we considered the possibility that a BZM+EGCG combination may result in the formation of a boronate adduct. However, in the presence of water and other hydroxylated molecules, these interactions could be formed reversibly, allowing both BZM and EGCG to exert their actions, despite the formation of this type of adduct.

Our studies³⁹ revealed that EGCG and other polyphenols instead of being synergistic, they effectively antagonized the apoptotic effects of BZM and significantly reduced its ability to induce cancer cell death *in vitro* and *in vivo*. The inactivation of BZM by green tea extracts was demonstrated in a number of experiments using the multiple myeloma cell line RPMI/8226

and U266, and the glioblastoma cell line LN229. These results illustrated a complete abrogation of BZM-mediated antitumor properties, with EGCG showing the most antagonistic effect. It was shown that this result was duplicated *in vivo* by exhibiting BZM's inactivation by EGCG in nude mice models implanted with multiple myeloma cells as well as in experiments using bone marrow isolated from multiple myeloma patients. Additional similar findings for BZM inactivation were also reported by others,^{63, 66-70} while one study⁷¹ showed that under certain conditions EGCG potentiates the effect of BZM.

We postulated³⁹ that the inactivation of BZM was the consequence of a covalent interaction to form a boronate adduct between the polyphenols and BZM. Some preliminary evidence for this transformation was obtained by ¹H NMR and ¹³C NMR, suggesting the formation of a new condensation product between the two compounds, that prevents covalent binding of the boronic acid group of BZM to the proteasome site.³⁹ Despite these findings, the significant variability in the inhibitory potency among the various polyphenols studied, did not fully account for the strong ability of EGCG to inactivate BZM. The condensation adducts of boronic acids with diols have been extensively investigated,^{8, 72, 73} and are well known to be formed reversibly. In principle, the boron adducts of polyphenols,^{67, 74, 75} can also behave similarly, further complicating the analysis of EGCG-mediated inactivation.

In order to gain additional insights regarding the effects of dietary polyphenols on the efficacy of BZM and potentially the growing number of other emerging boron-based drugs⁸⁻¹³ and diol-based pro-drugs,^{74, 76} the work reported in this paper was focused on a more detailed molecular characterization of the postulated BZM/EGCG boron adduct. Towards this goal we relied on a number of spectroscopic techniques and cell assays, in an effort to identify the key factors involved in this process.

Results

In our previous report on the inactivation of BZM by EGCG,³⁹ we provided direct evidence that the BZM/EGCG combination generates a new molecular entity, evidenced by the appearance of new peaks in ¹H and ¹³C NMR. While these data confirmed the formation of a new BZM/EGCG adduct, it was not possible to fully characterize this species without additional studies.

EGCG contains three polyphenol rings (A,B,D), two of which contain three adjacent hydroxyl groups, generating a number of possibilities for forming adducts with the boronic acid group of BZM. Moreover, the BZM/EGCG adduct could involve the formation of a neutral boronate adduct or an anionic borate group involving the participation of a third oxygen substituent at the boron. Additionally, the conversion of boronic acids to boronate or borate adducts with diols is a reversible process, depending on the conditions and the relative stability of the boron adducts. Thus, in order to fully compare the relative stability and physiological relevance of adducts such as the one formed from BZM and EGCG, it is important to determine the equilibrium constant of this transformation.

Therefore, in order to elucidate the key structural features of the BZM/EGCG adduct we relied on several NMR techniques, modeling studies as well as cell-based assays.

Structure elucidation of the BZM/EGCG adduct by ¹H NMR

The 400MHz ¹H NMR spectra of BZM, EGCG, and the 1:2 BZM/EGCG combination were analyzed and all of the C-H chemical shifts of EGCG and BZM were fully assigned (Fig. 3A,B). Interestingly, the ¹H NMR spectrum of the BZM/EGCG combination revealed several new peaks (Fig. 3C) that could be attributed to two isomeric adducts **9** and **10** (Fig. 3D).

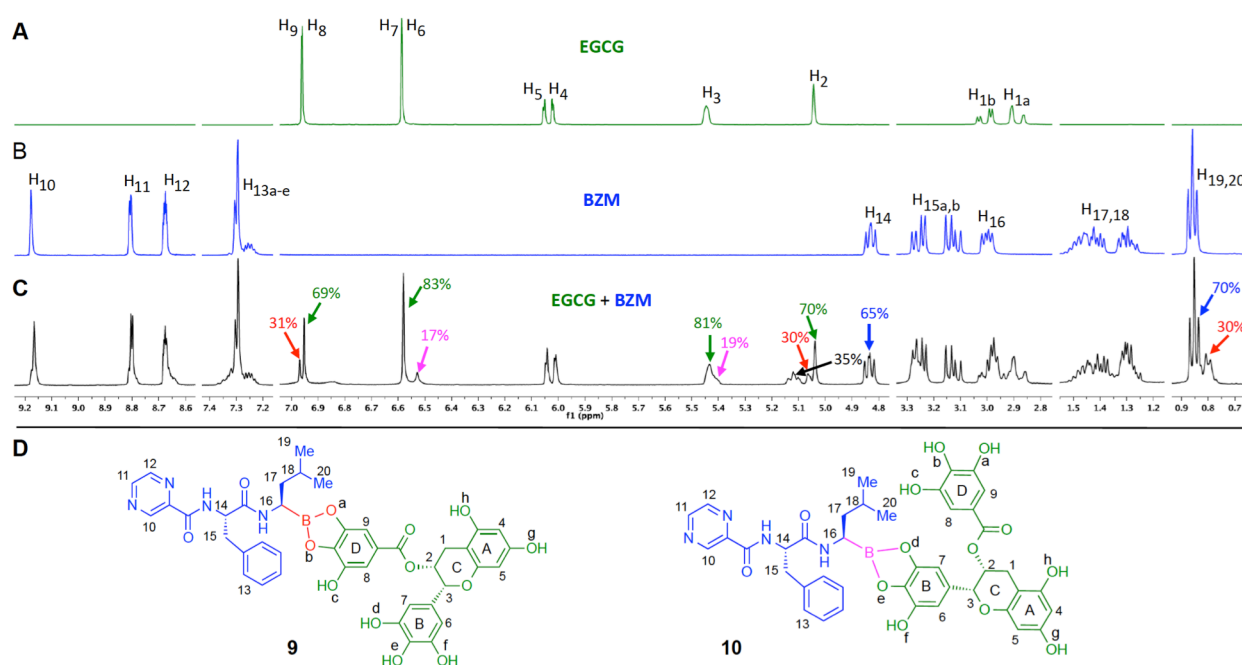


Fig. 3 A. 400MHz ¹H NMR of EGCG in MeCN; B. 400MHz ¹H NMR of Bortezomib (BZM) in MeCN; C. 400MHz ¹H NMR of 1:2 mixture of EGCG:BZM in MeCN; D. Postulated structures of boronate adducts (**9**, **10**) suggested by ¹H NMR analysis. Arrows indicate proton shifts corresponding to adducts of EGCG and BZM. Percentages indicate relative ratios of designated peaks.

The presence of new boron adducts such as **9**, involving the condensation of the boronic acid group of BZM with the gallic acid unit of EGCG (ring D), was suggested by two new downfield peaks resulting from deshielding of EGCG protons H₉ and H₂. This deshielding is consistent with the formation of a new O-B bond with oxygen atom O_a adjacent to H₉, resulting in the reduction of the electron donating effect of this phenolic OH of EGCG. A similar deshielding effect, involving a reduced electron donating effect by oxygen atom O_b towards the ester carbonyl, can explain the new downfield peak for H₂. Presumably, the O_b-H group in in EGCG is the most acidic due to its conjugation with the carboxyl ester and would exist as an anion in solution, while in adduct **9** oxygen O_b is more electron deficient due to its bonding to the boron atom. Notably, integration of the new peaks for both H₉ and H₂ revealed similar ratios in comparison with unreacted EGCG, namely 31:69 and 30:70 respectively (Fig. 3C). Comparable ratios of 30:70 and 35:65 were also observed for BZM at a new upfield peak for methyl groups H₁₉ and H₂₀ and a new downfield peak for H₁₄ respectively. The differentiation of these diastereotopic methyl groups in the BZM/EGCG adduct is expected, due to the greater barrier of rotation adjacent to the boron atom.

The ¹H NMR spectrum of the BZM/EGCG adduct also indicated two new upfield peaks adjacent to protons H₆ and H₃ with a ratio of 83:17 and 81:19, respectively. These peaks suggest the presence of a second type of BZM adduct **10**, formed by the condensation of the boronic acid of BZM with the pyrogallol moiety of EGCG (ring C). The shielding of both H₆ and H₃ in **10** is consistent with the presence of an anionic oxygen atom O_f, presumably due to bond formation between oxygen atoms O_d and O_e and the boron atom.

Quantification and structural analysis of the BZM/EGCG adduct by ¹¹B NMR

Although the ¹H and ¹³C NMR spectra of the BZM/EGCG combination revealed evidence for the formation of a boron adduct, these techniques are not adequate for determining the equilibrium constant of this interaction. The ¹H NMR shows multiple overlapping and poorly resolved peaks, while the most affected H-atoms are located at a distance, limiting the precise characterization of the boron unit. Additionally, the limited sensitivity of ¹³C NMR requires that the experiments be carried out at higher concentrations. However, since equilibrium constants are a function of concentration, these conditions do not accurately portray the formation of the boron adduct in physiologic conditions. Moreover, due to the high dilution and reversible nature of the BZM/EGCG adduct, liquid chromatography mass spectrometer analysis results in the break-up of this adduct.

In order to overcome the above challenges, we identified ¹¹B NMR as a better technique that allows studies at relevant concentrations and simplifies the analyses by focusing on the lone boron atom that connects BZM and EGCG. The ¹¹B NMR spectrum of BZM shows a broad downfield peak at 27.8 ppm for the trigonal boronic acid group (Fig. 4A, peak **a**). When combined with increasing concentrations of EGCG, the boronic

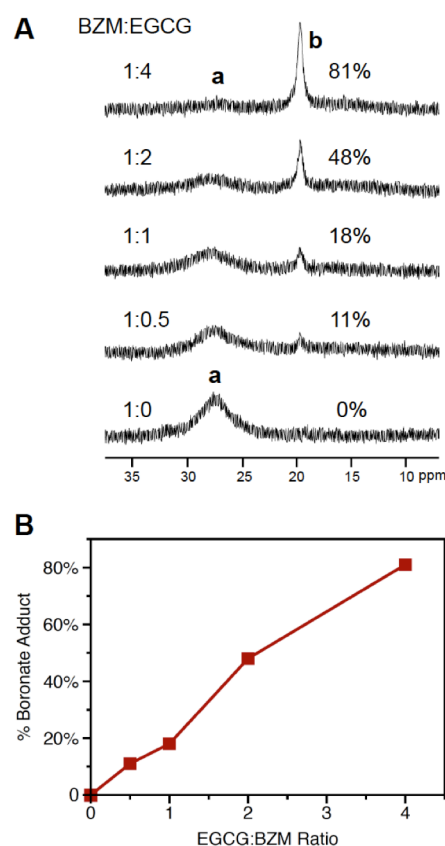


Fig. 4 (A) ¹¹B NMR in 4:1 CD₃CN/D₂O of the combination of BZM and EGCG in molar ratios of 1:0, 1:0.5, 1:1, 1:2, and 1:4 BZM:EGCG. The free boronic acid of BZM has a broad peak **a** at 27.8 ppm, while this peak is shifted to a narrow boronate peak **b** at 19.5 ppm. (B) Increased formation of the boronate adduct with the ratio of EGCG:BZM, determined by integration of the two boron peaks in ¹¹B NMR.

acid group is condensed with a diol moiety from EGCG resulting in a growing fraction of a new narrow upfield boron peak at 19.5 ppm (Fig. 4A, peak **b**). Interestingly, given its shielded position and narrow shape, peak **b** is unlikely to be from a simple trigonal cyclic boronate adduct, such as **9** or **10** (Fig. 3). Presumably, peak **b** provides direct evidence of an as-yet-unknown BZM adduct between BZM and EGCG. Thus, unlike ¹H and ¹³C NMR spectra (Fig. 3), ¹¹B NMR provides a simple, direct, and more accurate characterization of the BZM/EGCG adduct and the nature of the boron group.

Integration of the ¹¹B peaks allowed us to quantify the percentage of the BZM/EGCG adduct relatively to free BZM in solution (Fig. 4A). As we had shown by ¹H NMR (Fig. 3) and by ¹³C NMR,³⁹ EGCG readily creates a boron adduct with BZM in a concentration dependent manner (Fig. 4B). At a 4:1 EGCG to BZM ratio the free BZM was reduced significantly.

Comparison by ¹¹B NMR of selected polyphenols for their ability to form boron adducts with BZM

While EGCG was shown to be the most potent among related natural polyphenols for the inactivation of BZM, the basis of this activity remains unclear. In order to determine the

molecular characteristics of EGCG responsible for its high potency, we employed the above ^{11}B NMR approach to selected phenolic compounds with variable substitution patterns (Fig. 5).

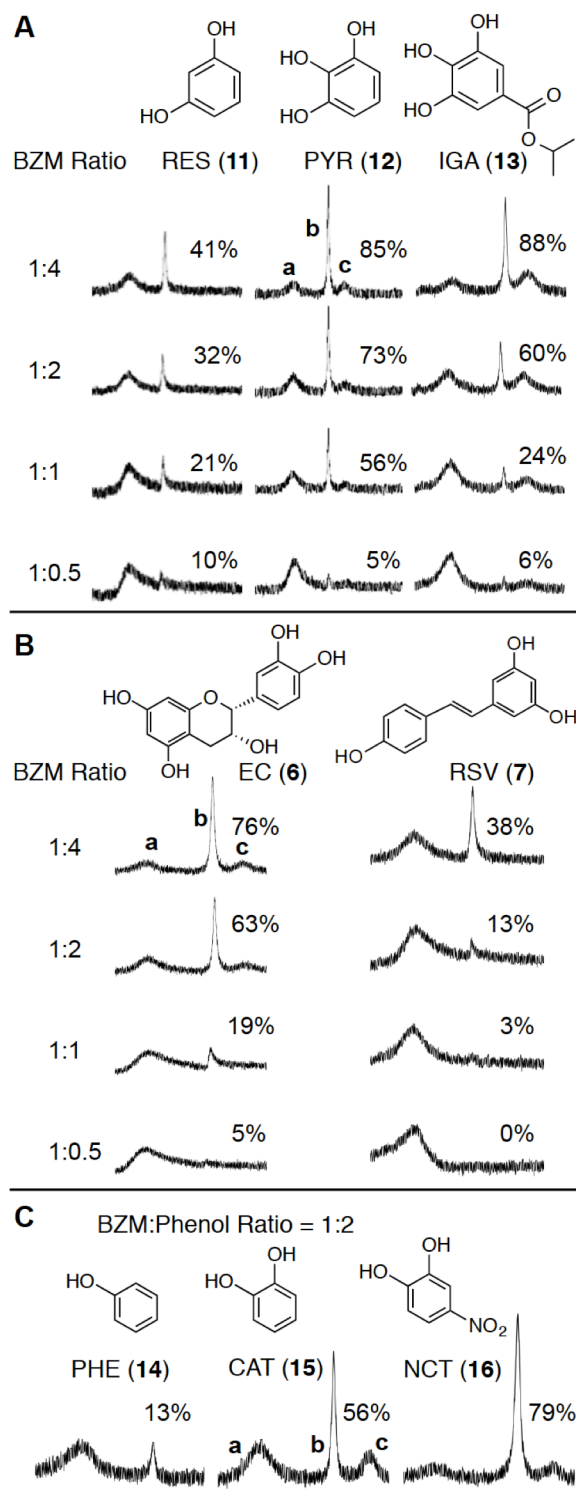


Fig. 5 The ^{11}B NMR of the adduct of BZM with increasing molar ratios of selected polyphenols was evaluated by integrating the boron peaks of BZM in combination with each of the following compounds: (A) Three polyphenols (RES, PYR, IGA) representing EGCG fragments. (B) The natural polyphenols (-)-epicatechin (EC) and resveratrol (RSV). (C) Phenol (PHE), catechol (CAT) and 4-nitro-catechol (NCT).

Thus, EGCG was divided into three fragments representing its three phenolic moieties (rings A,C,D): the 1,3-diol resorcinol (11, RES), the 1,2,3-triol pyrogallol (12, PYR), and the isopropyl gallate (13, IGA). The ^{11}B NMR of BZM by doubling the ratio of RES, PYR, IGA are shown in Fig. 5A.

PYR and IGA effectively formed the boronate adduct peaks **b** and **c** (Fig. 5A) at a 4:1 ratio to BZM, where the two adducts combined reached 85% and 88%, respectively. RES showed a decreased capacity to form a boronate adduct, with the majority of BZM remaining as the boronic acid. Since the m-substitution pattern of RES does not allow the formation of a cyclic BZM boronate, one of its hydroxyl groups forms a hydrolytically labile boronate monoester or boronate diester (see Fig. 9).

The above trends were further examined by comparing the ^{11}B NMR spectra of two dietary polyphenols, namely (-)-epicatechin (6, EC) and resveratrol (7, RSV) that contain 1,3- and/or 1,2-diol moieties respectively (Fig. 5B). Based on the 1,3-position of RSV's hydroxyl groups it was expected that this polyphenol would not readily complex with BZM, while the epicatechin (EC), which contains a 1,2-diol would be able to form a stable adduct at the 1:4 molar ratio with BZM. This was indeed confirmed (Fig. 5B).

Although the ^{11}B NMR of all of the BZM/polyphenol adducts (Fig. 5A,B) had the two boron peaks at 27.8 ppm (peak **a**) and 19.5 ppm (peak **b**) observed for the BZM/EGCG adduct (Fig. 4A), in some cases (PYR, IGA, EC) a third upfield and broad boron peak was observed at 15.8 ppm (peak **c**). To further investigate the factors leading to the formation of this additional boron adduct, we studied the ^{11}B NMR spectra of the BZM adducts of the parent phenol (14, PHE), catechol (15, CAT), and 4-nitrocatechol (16, NCT). As shown in Fig. 5C, the 1,2 diols CAT and NCT did have this third peak (**c**) with variable intensity, while PHE and RSV that lack a 1,2 diol did not. Taken together, these data indicate that the third peak **c** is likely to reflect the formation of a stable anionic cyclic borate species from a catechol (1,2-diol) moiety (e.g. 25, Fig. 9).

Interestingly, peak **c** was not observed in the ^{11}B NMR of the BZM/EGCG adduct, even though EGCG has multiple 1,2-diol moieties in its structure. Presumably, as discussed below, the more complex structural features of EGCG may prevent the formation of this type of anionic cyclic borate adduct.

Determination of the equilibrium constant of the BZM boron adduct by ^{11}B NMR and ^{19}F NMR

To further validate the applicability and accuracy of using ^{11}B NMR to evaluate the BZM/EGCG adduct, we sought to compare our ^{11}B data with related data generated by ^{19}F NMR. The use of ^{19}F NMR for studying biological systems⁷⁷ has been shown to be very effective in drug discovery⁷⁸ and for investigating protein function, including the calculation of binding constants in competition-based high throughput screening,^{79, 80} for screening enzyme inhibitors,⁸¹ and for determining the binding affinity of fluorinated molecules to protein targets. For example, we recently reported the effective use of ^{19}F NMR for estimating the equilibrium-binding constant of a benzamide derivative to the transcription factor MEF2.⁸²

In order to evaluate the BZM adduct with polyphenols we chose 4-fluorocatechol (**17**, FCT; Fig. 6) as our fluorine probe, where the single fluorine atom simplifies the ^{19}F NMR analysis to a single peak. For recording the NMR spectra, a 1:1 molar ratio of BZM and FCT were combined at a 2.6 mM concentration in a 1:1 ratio, and the experiment was run in triplicate. This experimental setup allowed the fraction of the unbound FCT to represent the concentration of both the free BZM and free FCT, which further simplified the calculation of the equilibrium constant. Moreover, both the ^{11}B and ^{19}F NMR spectra could be run on the same sample, providing a direct comparison of the two techniques.

Similarly to the ^{11}B NMR spectra of the BZM/CAT mixture, there were three peaks in the ^{11}B NMR for the BZM/FCT combination. The ^{19}F NMR spectra showed a narrow peak for FCT and a broad peak for the BZM/FCT boron adduct, presumably reflecting the two forms of the adduct. From these data, we calculated the binding constant of BZM/FCT at a 2.6 mM concentration to be 1.40×10^{-2} (± 0.002) M^{-1} by ^{19}F NMR, and 1.40×10^{-2} (± 0.006) M^{-1} by ^{11}B NMR (Fig. 6). The high degree of agreement between these methods indicates that ^{11}B NMR data would be useful for the calculation of equilibrium constants for BZM/polyphenol adducts.

Therefore, we applied the ^{11}B NMR method for the BZM/EGCG adduct. Using the same procedure as above, the calculated equilibrium constant for the formation of the BZM/EGCG boronate adduct was determined to be 3.40×10^{-2} (± 0.002) M^{-1} in a 2.6 mM solution. At molar concentrations of 1:1 of BZM and EGCG the equilibrium constant is less than 1, indicating that at 1:1 ratio the equilibrium favors reactants over adduct formation, in agreement with the above data (Fig. 4). Since EGCG is being consumed at much higher levels than BZM (g vs mg), and given the stability of the BZM/EGCG adduct, this equilibrium constant is biologically significant.

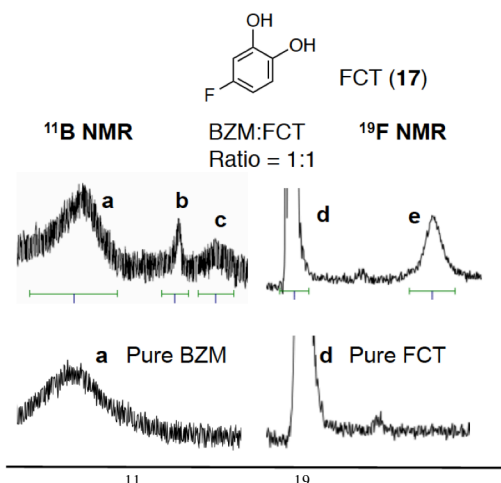


Fig. 6 Use of ^{11}B NMR and ^{19}F NMR to calculate the equilibrium constant of the boron adduct of 4-fluorocatechol (FCT, **17**) with BZM. These experiments were performed in triplicate (1-3) at a 2.6 mM concentration of a 1:1 mixture of BZM and FCT. The ratios of BZM/FCT were quantified by integrating the ^{11}B NMR peaks of BZM at 29 ppm (**a**) and the adduct at 19.7 ppm (**b**) and 16.4 ppm (**c**), as well as the ^{19}F NMR peaks of FCT at -124.9 ppm (**d**) and the adduct at -125.7 ppm (**e**).

Cell-based evaluation of the ability of EGCG and other phenols to affect the cytotoxic activity of BZM towards cancer cells

In order to correlate the ability of phenolic compounds to form boron adducts with BZM in relation with their ability to block BZM-mediated antitumor activity, we tested these compounds using *in vitro* assays. The anticancer activity of BZM alone and in combination with a series of structurally relevant phenolic compounds was evaluated in the multiple the myeloma cell line RPMI8226. Each compound was tested with an MTT assay at a concentration escalation of 0-40 μM in the absence or presence of 20 nM of BZM. After 48 hours of treatment with 20 nM of BZM alone, no proliferation of RPMI8226 was detected.

As reported previously,³⁹ increasing concentrations of EGCG (**3**) was able to ameliorate the cytotoxic effects of BZM against RPMI8226 cells with up to 82% (Fig. 7). The 1,2,3 tri-phenols PYR (**12**) and IGA (**13**) also exhibited potent inhibition of BZM-mediated anticancer activity in the RPMI8226 cell line at 40 μM (Fig. 7). Thus, the somewhat greater affinity observed for PYR vs IGA binding to BZM (Fig. 5) was also reflected by a similarly improved potency of the cytoprotective effect of PYR vs IGA in the RPMI8226 cells. Moreover, the compounds that had diminished ability to form a BZM adduct, including the mono-hydroxy PHE (**14**), the 1,3-diol RES (**11**), and resveratrol (RSV, **7**), all had no effect on cell viability in the presence of BZM. Among the catechols, CAT (**15**), FCT (**17**) and EC (**6**) showed moderate reduction of BZM activity, while NCT (**16**), which had a modest amount of the third peak **c**, showed almost no effect in cell viability (Fig. 7).

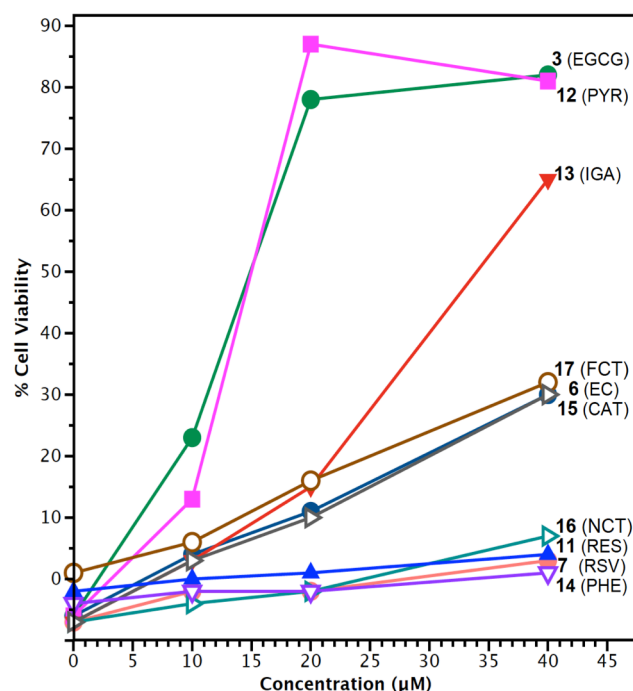


Fig. 7 Effects of EGCG and phenolic compounds on RPMI8226 cell viability in the presence of BZM. Percentage cell viability was determined via MTT assay after 48 hours of treatment with 0-40 μM of each compound in the presence of 20 nM BZM.

Discussion

The data reported above offer new insights on the molecular basis for the formation of stable boron adducts between BZM and polyphenols. By using several spectroscopic techniques, including ^1H NMR, ^{11}B NMR and ^{19}F NMR, and by comparing the BZM adducts of selected polyphenols we identified several structural aspects that can affect the formation and type of these boron adducts.

Molecular characteristics of the BZM-proteasome adduct

The biological actions of BZM result from its ability to bind selectively and reversibly to the chymotrypsin-like active site of the catalytic 20S proteasome component of the 26S proteasome.¹⁷ The key binding interactions of BZM to its target have been elucidated crystallographically (Fig. 8A).⁸³ It was shown that BZM forms a covalent anionic borate adduct with the hydroxyl group of Thr1 of the $\beta 5$ subunit of the proteasome. This borate group is further stabilized via hydrogen bonds of its two hydroxy groups with the amino groups of Thr1 and Lys33. Additional hydrogen bond interactions occur with four active site residues of the $\beta 5$ subunit (Thr21, Gly47, Ala49, Ala50), and with Asp114 of the $\beta 6$ subunit bridged with a water molecule (Fig. 8A,B).⁸³ Overall, these interactions explain the potency and specificity of BZM, as well as the reversible nature of the BZM/proteasome adduct. They may also explain the observed affinity of certain polyphenols to form BZM adducts.

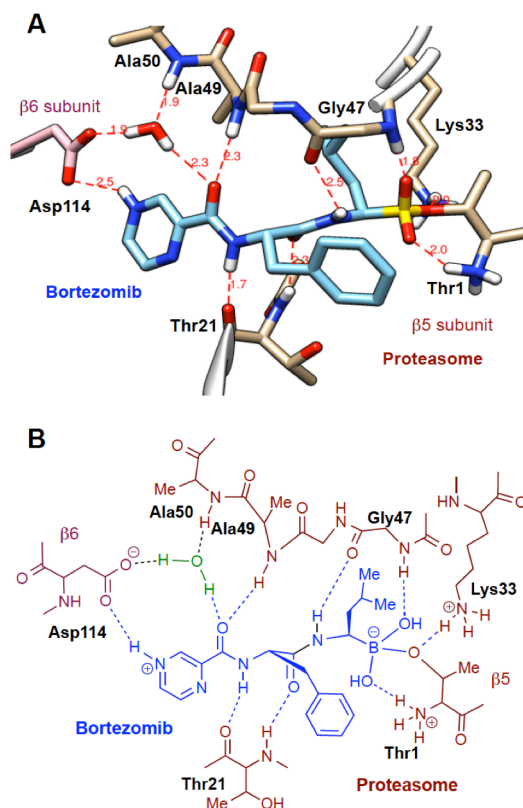


Fig. 8 Molecular interactions of BZM with key residues of the proteasome active site. (A) Model adapted from the crystal structure of BZM bound to proteasome 20S (PDB: 2F16). (B) Contacts between BZM and proteasome active site residues.

Due to the Lewis hard-soft acid-base principle, the boronic acid of BZM shows a greater affinity to hard oxygen atoms (e.g. Thr OH) than to soft sulfur atoms (e.g. Cys SH).⁸³ The same principle would be helpful in interpreting the observed BZM affinity among polyphenols, where modulation of the electronic properties of binding oxygen atoms can affect the formation and stability of the boron adduct. Moreover, any factors that affect the acidity of particular phenolic OH groups can also affect the overall reactivity of polyphenols.

Reversibility of boron adduct formation from BZM and phenols

The reaction of boronic acids with alcohols and diols is typically a facile and reversible process that involves the formation of a number of boronate (trivalent B) and borate (tetraivalent B) adducts. The relative stability of these boron adducts can be significantly affected by both electronic and steric factors. In order to compare the formation of BZM adducts among various polyphenols, we postulated the detailed reversible steps summarized in Fig. 9.

Reaction of BZM (**1**) with phenol (PHE, **14**) or phenoxide (**18**) initially forms a borate monoester (**19**) that can be readily converted to the boronate monoester (**20**), and eventually to the corresponding boronate diester (**21**). Similar reactivity is expected for 1,3 diols (RES, **11**; RSV, **7**). However, this process is significantly altered if the phenolic compound is a 1,2-diol (catechol) or a 1,2,3-triol (pyrogallol). Thus, reaction of BZM with a catechol (**22**) initially forms a borate monoester adduct (**23**), which is ideally suited for a fast intramolecular deprotonation of the second phenolic OH group to form a boronate monoester (**24**). The anionic phenoxy moiety of **24** is expected to undergo a fast intramolecular binding to the boron atom to form an anionic cyclic borate (**25**). Finally, acid-base reaction among borate OH group and another phenolic OH can lead to the formation of neutral cyclic boronate **26**.

Since all of the above steps are generally reversible, the boron adducts that accumulate in solution under equilibrium conditions are those that have greater thermodynamic stability. Moreover, if any of these steps have high kinetic barriers the equilibrium conditions will require higher temperatures or longer equilibration times.

Differences in boron adduct formation from BZM and phenols

We postulate that all BZM-derived borates, including **19**, **23** and **25**, can be further stabilized via an intramolecular hydrogen bond with the adjacent amide group of BZM (Fig. 9). This type of hydrogen bond is analogous to the intramolecular hydrogen bond between Gly47 of the proteasome and one of the hydroxy groups of the borate monoester adduct of BZM (Fig. 8).

However, unlike the proteasome-bound BZM borate, which is further stabilized by two additional intramolecular hydrogen bonds with the ammonium groups of Thr1 and Lys 33 (Fig. 8), borate monoesters of type **19** are expected to be more labile and either readily reverse to the BZM boronic acid or be converted to a boronate monoester **20** or a boronate diester **21**. This hypothesis is consistent with the observed lack of any borate adduct peaks in the ^{11}B NMR of mono-phenolic compounds

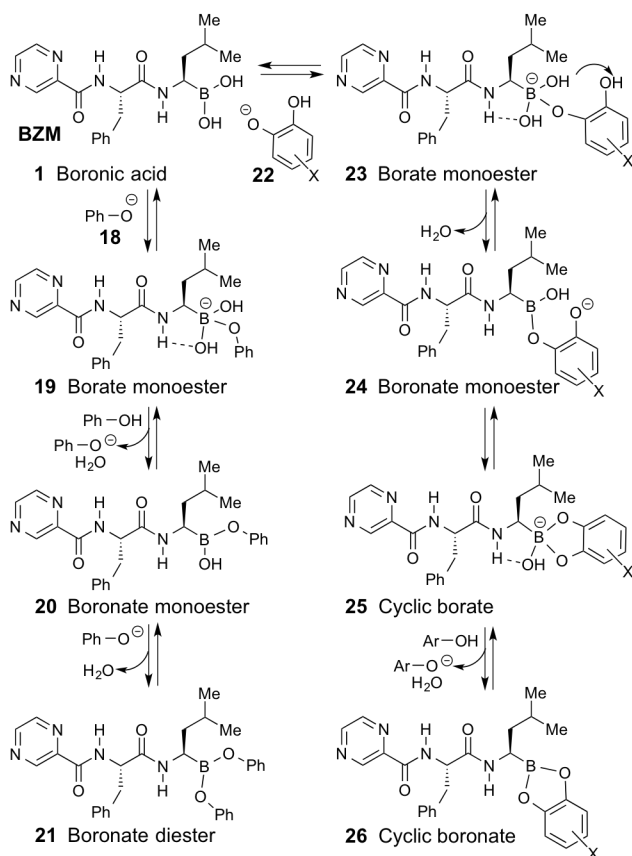


Fig. 9 Condensation of BZM with phenolic compounds to form boronate and borate adducts. All steps are reversible depending on the conditions and the relative stability of these borate and boronate adducts.

such as PHE (14), RSV (7) and RES (11), shown in Fig. 5. This is consistent with the lack of any inhibition of BZM-mediated activity against cancer cells by mono-phenols (Fig. 7).

The kinetic and thermodynamic factors are quite different for the formation of BZM boron adducts with 1,2-diols or 1,2,3-triols. The intramolecular conversion of borate 23 to anionic boronate 24 is expected to be entropically favored and to have a low kinetic barrier. Similarly, the intramolecular conversion of 24 to cyclic borate 25 is also expected to be a generally facile process. Assuming that the borate OH group of 25 is stabilized via an intramolecular hydrogen bond as described above, and given its more sterically hindered position, this means that the formation of borate 25 can be favored both kinetically and thermodynamically.

Indeed, this hypothesis is consistent with the observed accumulation of a borate peak in the ^{11}B NMR of the BZM adducts with the 1,2-diols EC (6), CAT (15), NCT (16), FCT (17), and the 1,2,3-diols PYR (12) and IGA (13), as shown in Figs. 5 and 6. This is also consistent with the fact that catechols having electro-withdrawing groups (e.g. NCT, 16) showed increased boronate but reduced borate adduct formation, presumably due to the greater stability of the anionic boronate 24, the precursor of 25. Although the condensation of boronic acids with 1,2-diols is known to be sensitive to substituent

effects and varies with the pH, these general binding affinity trends are more complex and not always true.⁷³

The postulated relative stability of 24 and 25 depending on their substitution patterns is also consistent with the observed relative potency of the various 1,2-diols and 1,2,3-triols to inhibit the activity of BZM (Fig. 7). Thus, the most electron rich phenolic 1,2,3-triols and IGA (13) were also the most potent. The ability of PYR (12) and its analogs to form stable boronate adducts was also attributed to its potent antibacterial properties by antagonizing bacteria quorum sensing, which is mediated by the formation of a borate species.⁸⁴

Similarly, the 1,2-diols EC (6), CAT (15), and FCT (17) had moderate activity, while the nitro-catechol (NCT, 16) bearing a strong electronegative group had no activity, despite the formation of a large and sharp upfield peak, similarly to EGCG (Fig. 5C). This outlier behavior of NCT may be due to the formation of an unusual BZM adduct. Thus, due to its more anionic nature (22) it can form more reversibly an anionic boronate monoester intermediate with BZM (24). By not being converted to a stable cyclic borate 25, the monoester NCT intermediates 22 and 24 are more readily reverted to NCT and BZM, resulting in reduced interference on BZM activity. Even if NCT does form an anionic tetrahedral cyclic borate (25), the presence of the strongly electronegative nitro group would readily revert 25 back to 24 rather than lead to 26. Alternatively, it is possible that NCT does indeed form a stable BZM adduct analogously to EGCG, but its inability to increase cell viability despite blocking BZM may be due to its own cytotoxic properties or to its own metabolic deactivation.

Overall, phenolic compounds capable of forming stable cyclic borate or cyclic boronate BZM adducts that are more stable than the binding of BZM to the proteasome (Fig. 8), would be more potent inhibitors of BZM activity.

Unique molecular characteristics of the BZM/EGCG adduct

Although EGCG contains the same phenolic groups as RES, PYR, IGA, the ^{11}B NMR of BZM/EGCG adducts 9 and 10 (Fig. 4) did not show the formation of borate adduct similarly to PYR and IGA (peak c, Fig. 5). The absence of a borate species can be attributed to steric reasons, and it gives insight as to how and why EGCG is such a potent inhibitor of BZM. The NMR data reported above revealed several molecular features of EGCG that may be responsible for these actions (Fig. 10)

The boronic acid group of BZM (1) is attached to a saturated carbon, and therefore its boron atom is highly electrophilic and in the presence of water it likely exists as a solvated species (1a, Fig. 10). Also, the most acidic phenolic hydroxyl group of EGCG (3) is at the p-position to the gallate ester (i.e. at O_b), and it is likely to exist as a solvated phenoxide anion (3a). Therefore, O_b would be favored to react with BZM to form the trigonal boronate monoester 27. As outlined in Fig. 10, intermediate 27 will be readily converted to the tetrahedral cyclic borate 28, which can then form a cyclic boronate group (e.g. 9 Fig. 3) as the major component of the BZM/EGCG adduct. The loss of the anionic OH group from borate 28 is

presumably facilitated by reaction with water and/or an adjacent phenolic OH in EGCG (Fig. 10).

The ^1H NMR of the BZM/EGCG adduct (Fig. 3) showed that protons H_2 as well as H_8 and/or H_9 of EGCG and proton H_{14} of BZM shifted downfield, while one or both of the two methyl groups of BZM (H_{19} , H_{20}) shifted upfield. These data are consistent with a more rigid structure and the presence of an additional intramolecular interaction among the boron atom and the carbonyl oxygen of the adjacent amide bond, as illustrated in structure **9a** (Fig. 10). This structure has an increased electronic density at the boron atom that may explain the shielding of the methyl groups (H_{19} , H_{20}). Structure **9a** is also consistent with the differentiation of H_8 and H_9 . Although in the postulated structure **3a** of unreacted EGCG both O_a and O_c cause equal shielding of H_8 and H_9 , in the BZM/EGCG adduct **9a** only O_c becomes more anionic, resulting in the selective shielding of H_8 while H_9 remains unshielded and is represented by the observed downfield shift. Moreover, structure **9a** is consistent with the observed downfield shift of H_{14} , resulting from the increased positive charge at the adjacent amide bond.

The formation of an intramolecular adduct such as **9a**

instead of the cyclic borate **28**, which was not observed in the ^{11}B NMR, may be the result of the larger size and more complex nature of EGCG. When it binds with BZM the surrounding bulk of this complex polyphenol provides steric hindrance for the cyclic borate group, and also limits solvation by the aqueous medium. Loss of the OH group from the crowded borate **28** leads to the less hindered cyclic boronate **9**, which adopts the more stabilized neutral borate structure **9a**.

Similar factors can explain the formation of the BZM/EGCG adduct at the pyrogallol ring of EGCG (**10a**, Fig. 10). Initial formation of boronate monoester **29** leads to the cyclic borate **30**, which is converted to the intramolecularly stabilized cyclic boronate **10a**. This structure is consistent with the observed upfield shift in H_3 and H_6 resulting from the more anionic nature of O_e and O_f in **10a** in comparison with EGCG. It may also account for the increased ratio (35:65) of the downfield shifted BZM proton H_{14} (Fig. 3).

Structures **9a** and **10a** are consistent with the postulated as-yet-unknown boron species suggested by the ^{11}B NMR of the BZM/EGCG adduct (Fig. 4). Unlike the trigonal boronic acid group of BZM, having a broad downfield ^{11}B peak at 27.8 ppm,

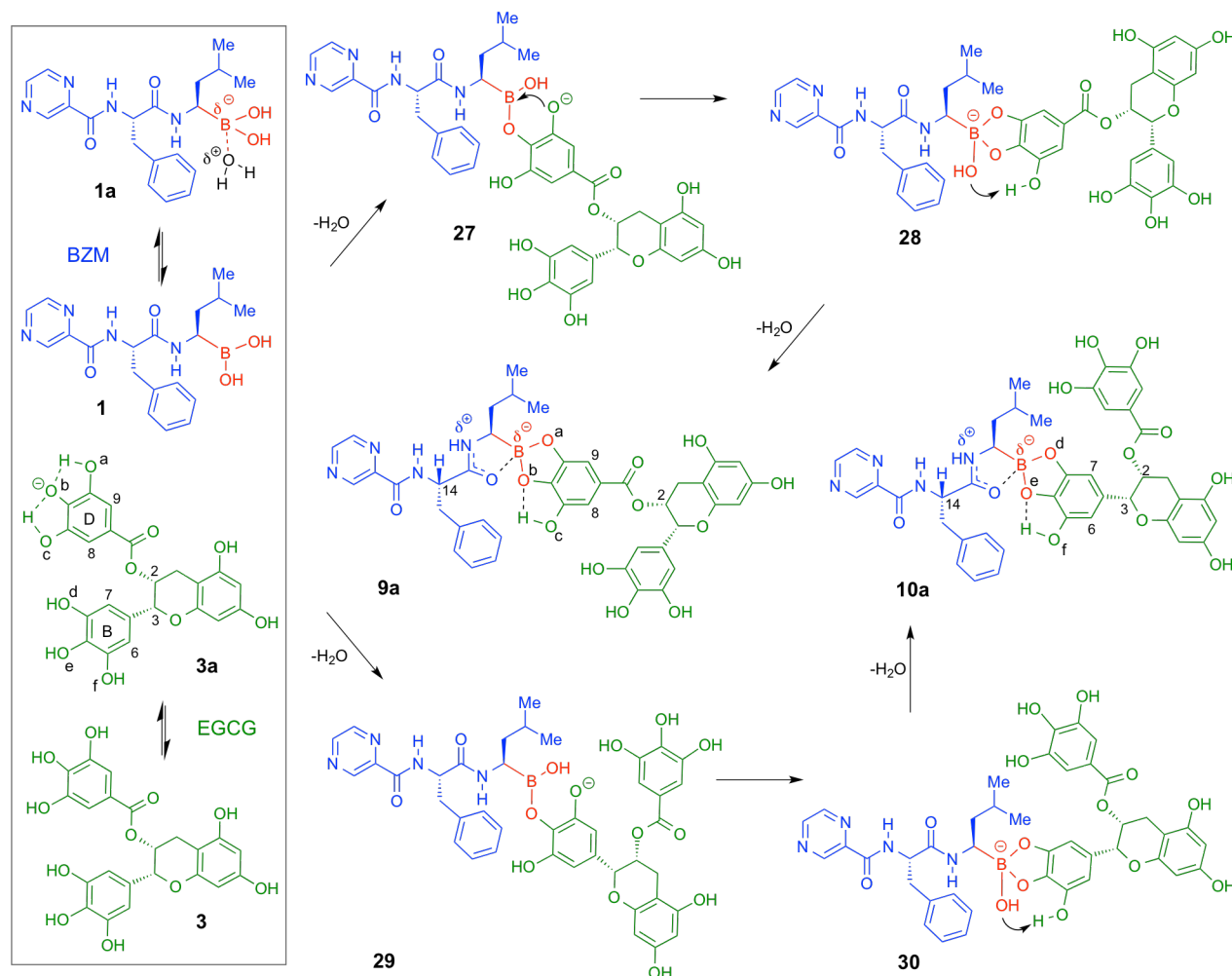


Fig. 10 Postulated molecular mechanism for the condensation of BZM with EGCG to form the stable boron adducts **9a** and **10a**. The formation of the major BZM/EGCG adduct **9a** is initiated at the more anionic EGCG gallate ring D and sequentially results in the formation of intermediates **26** and **27**, which is irreversibly converted to the intramolecularly stabilized boron adduct **9a**. A similar sequence initiated at the pyrogallol ring B leads to intermediates **28** and **29**, which is converted to the similar boron adduct **10a**.

the intramolecularly stabilized and polarized tetrahedral boron groups of **9a** and **10a** can account for the narrow upfield ^{11}B peak at 19.5 ppm. Moreover, the broad upfield ^{11}B peak at 15.8 ppm observed for BZM adducts of catechol or pyrogallol components (Fig. 5) is consistent with the tetrahedral anionic cyclic borates **25** (Fig. 9). All of these stable BZM adducts (**9a** / **10a** and **25**) result from a catechol cyclic boronate species (**26**, Fig. 9), which has a boron atom with increased Lewis acidity.

Presumably, for EGCG the intramolecular coordination of the oxygen atom of the adjacent amide bond of BZM to the electrophilic boronate group leads to the electronically and sterically stabilized BZM/EGCG adducts **9a** and **10a**, which would be resistant to hydrolysis. These novel intramolecular borate species are similar to the *N*-methyliminodiacetic acid boronate (MIDA) adducts, which are also very stable and have narrow upfield ^{11}B NMR peaks.⁸⁵

Among EGCG components, only PYR was as potent as EGCG in blocking BZM's activity, while IGA was less active, and RES was inactive (Fig. 7). While the greater potency of PYR may suggest that the PYR-containing ring B would be the EGCG site for the major boron adduct formation (i.e. boron adduct **10**), this does not seem to be the case. As suggested by the ^1H NMR of a 1:2 ratio of BZM/EGCG (Fig. 3), the major product is boron adduct **9** or **9a**, formed at the gallate-type ring D, which contains a carboxylic ester group. Presumably, the electron-withdrawing carbonyl group increases the acidity of the *p*-phenolic OH group of O_b , and the resulting anionic moiety **3a** facilitates the formation of a new O-B bond with BZM's boronic acid. Therefore, the preferred site for adduct formation (gallate ring D) is determined by the most acidic hydroxy group that would exist as an alkoxide anion (**3a**).

The inherent reversibility of boronic acid/diol adducts limits the effectiveness of the BZM polyphenol complexation. However in the case of EGCG and BZM the reversibility of this interaction is limited by the electronic properties of the polyphenol moieties and the steric bulk of the EGCG molecule. Once formed, boron adducts **9a** and **10a** would be harder to revert to the respective precursor borates **28** and **30** because it would be more difficult for an anionic hydroxide to access this crowded site. This is further illustrated in a molecular model comparison of EGCG (**3**) with the less hindered EC (**6**), as depicted in Fig. 11.

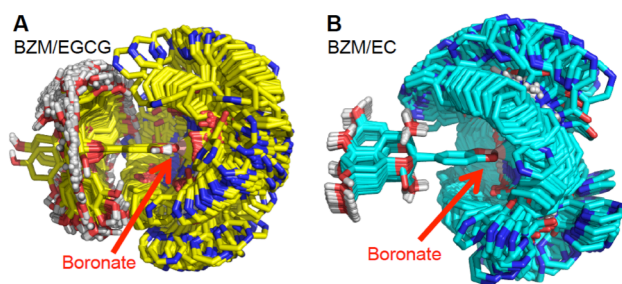


Fig. 11 Molecular modeling calculation and assessment of the BZM/EGCG boronate adduct (**A**) in comparison with the BZM/EC adduct (**B**) showing the lowest energy conformations. The BZM/EGCG boronate displays greater steric hindrance, while the BZM/EC boronate is more accessible and more stable.

Taken together, the observed properties of EGCG in inactivating BZM (Fig. 10) can be attributed to the following sequence: (a) selective formation of the BZM/EGCG anionic boronate monoesters **27** and **29**, respectively at the most acidic OH group of oxygen atom O_b at ring D, and the pyrogallol ring B; (b) fast intramolecular conversion of **27** and **29**, to anionic cyclic borates **28** and **30**; and (c) thermodynamically favored conversion of **28** and **30** to the less sterically hindered and intramolecularly stabilized tetrahedral neutral cyclic borate BZM/EGCG adducts **9a** and **10a**. After these novel adducts are formed, due to steric reasons and the inaccessibility of the boron group, they are more difficult to undergo hydrolysis back to their components, thereby limiting the availability of free BZM. This analysis is consistent with the lack of anionic borate formation in the ^{11}B NMR of the BZM/EGCG (Fig. 4), and the greater ability of these stable BZM adducts to limit the activity of BZM, as compared with other similar compounds (Fig. 7).

NMR evaluation of polyphenol adducts of boron drugs

The use of NMR spectroscopy to elucidate the type of boron adduct being formed (if any) provides a useful method for determining the potential ability of dietary polyphenol compounds to form undesired adducts with boron-based drugs and interfere with their actions. With the increasing interest in developing new therapeutics containing boronic acid groups,⁸⁻¹⁶ this comparative approach may have a broader applicability.

Conclusions

In summary, we have fully characterized the covalent boron adduct of BZM with the green tea extract polyphenol EGCG. Through the use of ^1H NMR, ^{11}B NMR and ^{19}F NMR, we characterized the structures of the BZM boron adducts of EGCG and related polyphenols, and investigated the factors contributing to their formation. We were also able to quantify the adduct formation and determine its equilibrium constant, which was found to be biologically significant.

The observed adducts included both neutral boronate and anionic borate derivatives, while their formation was preferably initiated at the most acidic phenolic OH group. The type and amount of the boron adduct produced is defined by both electronic and steric effects that can affect the reversibility of these steps. These structural characteristics were correlated with cell-based evaluation of the ability of EGCG and other phenols to suppress the anticancer activity of BZM.

In the case of EGCG, its ability to make a more stable adduct less reversibly with BZM seems to be due to two key factors: (a) electronic effects that drive the formation of boron adducts at the gallate ring D and the pyrogallol ring B, and (b) steric effects that favor the conversion of anionic cyclic borate species to intramolecularly stabilized neutral cyclic borate BZM/EGCG adducts, which are less susceptible to hydrolysis.

The reported approach provides a useful method for determining the potential ability of dietary polyphenol compounds to form undesired adducts with boron-based therapeutics and interfere with their actions.

Experimental

Materials

All commercially available products were used without further purification. Bortezomib (BZM) was purchased from LC laboratories as a free base. Epigallocatechin gallate (EGCG), pyrogallol (PYR), resorcinol (RES), catechol (CAT), phenol (PHE), 4-nitrocatechol (NCT), resveratrol (RSV), and (-)-epicatechin (EC) were all purchased from Sigma-Aldrich; 4-fluorocatechol (FCT) was purchased from Combi-Blocks.

Preparation of isopropyl gallate (IGA)

Gallic acid monohydrate (0.3 grams, 1.8 mmols), 1-ethyl-3-(3-dimethylaminopropyl)carbodiimide (0.341 grams, 2.2 mmols) (0.022 grams, 0.18 mmols) 4-dimethylaminopyridine in 5 mL of dry CH_2Cl_2 stirred at 0°C . Isopropyl alcohol (0.132 grams, 2.2 mmols) was added to the mixture and stirred for 30 minutes at 0°C then allowed to reach room temperature and stirred for another 48 hrs. The reaction mixture was quenched with sodium bicarbonate and extracted with ethyl acetate to yield pure isopropyl 3,4,5-trihydroxybenzoate (isopropyl gallate) as a tan powder (61% yield).

NMR Spectroscopy

NMR spectra were recorded on a Varian 500 2-channel NMR spectrometer with an Agilent OneNMR probe (^1H - $^{19}\text{F}/^{31}\text{P}$ - ^{15}N 5 mm PFG OneNMR probe) and a Varian 400 2-channel NMR spectrometer with an Agilent OneNMR probe (^1H - $^{19}\text{F}/^{31}\text{P}$ - ^{15}N 5 mm PFG OneNMR probe). Chemical shifts (δ) are expressed in parts per million (ppm). All the experiments were performed at 25°C . All samples were diluted to 1 mL in an 80% CD_3CN , 20% D_2O solvent system. For all samples 2.80 mg of bortezomib (7.3×10^{-3} mmols) and adequate quantity of phenol was added by mass and spun for 15 minutes at room temperature. All spectra were processed with MestReNova v9.0 software.

Cell lines and culturing

Human multiple myeloma cell line RPMI/8226 (ATCC® CCL-155™) was obtained from ATCC (Manassas, VA). MM cells were propagated in RPMI-1640 (Cellgro, Herndon, VA). Cells were grown with 10% fetal bovine serum, 100 U/mL penicillin, and 100 $\mu\text{g}/\text{mL}$ streptomycin (Gemini Bio-Products, West Sacramento, CA) in a humidified incubator at 37°C and a 5% CO_2 atmosphere.

MTT proliferation assay

MTT assays used multiple myeloma cells were performed using 96-well plates where 2.5×10^4 cells were added per well. Cells suspended in culture medium (50 $\mu\text{L}/\text{well}$) were seeded in 96-well plates and incubated for 24 hours in a humidified atmosphere of 37°C and a 5% CO_2 . Compounds were diluted with culture medium to various concentrations and fed to the culture. Cells were then incubated for 48 hours and were subsequently treated with MTT (10 $\mu\text{L}/\text{well}$, 5 mg/mL in phosphate buffered saline) and incubated for an additional 4 hours. Lysis buffer (10% SDS/0.1% HCl in deionized water, 100 $\mu\text{L}/\text{well}$) was added to each well, and the cells were incubated at room temperature for 17 hours in darkness. The

absorbance at 490 nm was measured by a microplate reader. In individual experiments, each condition was set up in triplicate.

Acknowledgements

This work was supported in part by the Zumberge Research and Innovation Fund of the University of Southern California and by the Arthur C. Cope Scholar Fund administered by the American Chemical Society. We thank the NSF (grants DBI-0821671, CHE-0840366) and the NIH (grant S10 RR25432) for funding the NMR spectrometers, and the NCI (grant P30CA014089) for support of other resources used in this study. We also thank Prof. T. J. Williams for his help with NMR data analysis.

Notes and references

- J. Adams, M. Behnke, S. Chen, A. A. Cruickshank, L. R. Dick, L. Grenier, J. M. Klunder, Y.-T. Ma, L. Plamondon and R. L. Stein, *Bioorganic & Medicinal Chemistry Letters*, 1998, **8**, 333-338.
- J. Adams, V. J. Palombella, E. A. Sausville, J. Johnson, A. Destree, D. D. Lazarus, J. Maas, C. S. Pien, S. Prakash and P. J. Elliott, *Cancer Research*, 1999, **59**, 2615-2622.
- P. G. Richardson, C. Mitsiades, T. Hideshima and K. C. Anderson, *Annual Review of Medicine*, 2006, **57**, 33-47.
- M. Cavo, *Curr Hematol Malig Rep*, 2007, **2**, 128-137.
- K. N. Utecht and J. Kolesar, *American Journal of Health-System Pharmacy*, 2008, **65**, 1221-1231.
- M. Curran and K. McKeage, *Drugs*, 2009, **69**, 859-888.
- N. A. Petasis, *Australian Journal of Chemistry*, 2007, **60**, 795-798.
- W. Yang, X. Gao and B. Wang, *Medicinal Research Reviews*, 2003, **23**, 346-368.
- D. G. Hall, ed., *Boronic Acids: Preparation, Applications in Organic Synthesis and Medicine*, Wiley-VCH Verlag GmbH & Co. KGaA, Weinheim, 2005, pp. 1-549.
- W. Yang, X. Gao and B. Wang, in *Boronic Acids: Preparation, Applications in Organic Synthesis and Medicine*, ed. D. G. Hall, Wiley-VCH Verlag GmbH & Co. KGaA, Weinheim, 2005, pp. 481-512.
- P. C. Trippier and C. McGuigan, *MedChemComm*, 2010, **1**, 183-198.
- S. J. Baker, J. W. Tomsho and S. J. Benkovic, *Chem. Soc. Rev.*, 2011, **40**, 4279-4285.
- R. Smoum, A. Rubinstein, V. M. Dembitsky and M. Srebnik, *Chem. Rev.*, 2012, **112**, 4156-4220.
- B. D. Dorsey, M. Iqbal, S. Chatterjee, E. Menta, R. Bernardini, A. Bernareggi, P. G. Cassarà, G. D'Arasmo, E. Ferretti, S. De Munari, A. Oliva, G. Pezzoni, C. Allievi, I. Strepponi, B. Ruggeri, M. A. Ator, M. Williams and J. P. Mallamo, *J. Med. Chem.*, 2008, **51**, 1068-1072.
- M. M. Seavey, L. D. Lu, K. L. Stump, N. H. Wallace and B. A. Ruggeri, *International Immunopharmacology*, 2012, **12**, 257-270.
- C. R. Berkens, Y. Leestemaker, K. G. Schuurman, B. Ruggeri, S. Jones-Bolin, M. Williams and H. Ovaa, *Molecular Pharmaceutics*, 2012, **9**, 1126-1135.
- S. Murata, H. Yashiroda and K. Tanaka, *Nat Rev Mol Cell Biol*, 2009, **10**, 104-115.
- J. Adams, *Drug Discovery Today*, 2003, **8**, 307-315.
- J. Adams, *Cancer Treatment Reviews*, 2003, **29**, 3-9.
- J. Adams, *Nat Rev Cancer*, 2004, **4**, 349-360.
- J. Adams, *Cancer Cell*, 2004, **5**, 417-421.
- B. S. Moore, A. S. Eustaquio and R. P. McGlinchey, *Current Opinion in Chemical Biology*, 2008, **12**, 434-440.
- T. Hideshima, H. Ikeda, D. Chauhan, Y. Okawa, N. Raje, K. Podar, C. Mitsiades, N. C. Munshi, P. G. Richardson, R. D. Carrasco and K. C. Anderson, *Blood*, 2009, **114**, 1046-1052.
- N. Rastogi and D. P. Mishra, *Cell Division*, 2012, **7**, 26.
- D. R. Fels, J. Ye, A. T. Segal, S. J. Kridel, M. Spiotto, M. Olson, A. C. Koong and C. Koumenis, *Cancer Research*, 2008, **68**, 9323-9330.
- L. Vincenz, R. Jäger, M. O'Dwyer and A. Samali, *Molecular Cancer Therapeutics*, 2013, **12**, 831-843.

27. J. J. Wright, *Clinical Cancer Research*, 2010, **16**, 4094-4104.
28. A. Kardosh, N. Soriano, Y.-T. Liu, J. Uddin, N. A. Petasis, F. M. Hofman, T. C. Chen and A. H. Schönthal, *Blood*, 2005, **106**, 4330-4338.
29. L. M. Backhus, N. A. Petasis, J. Uddin, A. H. Schönthal, R. D. Bart, Y. Lin, V. A. Starnes and R. M. Bremner, *J. Thorac. Cardiovasc. Surg.*, 2005, **130**, 1406-1412.
30. A. Kardosh, W. Wang, J. Uddin, N. A. Petasis, F. M. Hofman, T. C. Chen and A. H. Schönthal, *Cancer Biol. Ther.*, 2005 **4**, 571-582.
31. A. Kardosh, E. B. Golden, P. Pyrko, J. Uddin, F. M. Hofman, T. C. Chen, S. G. Louie, N. A. Petasis and A. H. Schönthal, *Cancer Research*, 2008, **68**, 843-851.
32. H.-Y. Cho, W. Wang, N. Jhaveri, S. Torres, J. Tseng, M. N. Leong, D. J. Lee, A. Goldkorn, T. Xu, N. A. Petasis, S. G. Louie, A. H. Schönthal, F. M. Hofman and T. C. Chen, *Molecular Cancer Therapeutics*, 2012, **11**, 2462-2472.
33. H.-Y. Cho, S. Thomas, E. B. Golden, K. J. Gaffney, F. M. Hofman, T. C. Chen, S. G. Louie, N. A. Petasis and A. H. Schönthal, *Cancer Letters*, 2009, **282**, 87-97.
34. N. Sharma, S. Thomas, E. B. Golden, F. M. Hofman, T. C. Chen, N. A. Petasis, A. H. Schönthal and S. G. Louie, *Cancer Letters*, 2012, **326**, 143-154.
35. S. Thomas, N. Sharma, E. B. Golden, H. Cho, P. Agarwal, K. J. Gaffney, N. A. Petasis, T. C. Chen, F. M. Hofman, S. G. Louie and A. H. Schönthal, *Cancer Letters*, 2012, **325**, 63-71.
36. P. Pyrko, N. Soriano, A. Kardosh, Y.-T. Liu, J. Uddin, N. Petasis, F. Hofman, C.-S. Chen, T. Chen and A. Schönthal, *Molecular Cancer*, 2006, **5**, 1-16.
37. P. Pyrko, A. Kardosh, Y.-T. Liu, N. Soriano, W. Xiong, R. H. Chow, J. Uddin, N. A. Petasis, A. K. Mircheff, R. A. Farley, S. G. Louie, T. C. Chen and A. H. Schönthal, *Molecular Cancer Therapeutics*, 2007, **6**, 1262-1275.
38. H.-C. Chuang, A. Kardosh, K. J. Gaffney, N. A. Petasis and A. H. Schönthal, *Molecular Cancer*, 2008, **7**, 1-13.
39. E. B. Golden, P. Y. Lam, A. Kardosh, K. J. Gaffney, E. Cadenas, S. G. Louie, N. A. Petasis, T. C. Chen and A. H. Schönthal, *Blood*, 2009, **113**, 5927-5937.
40. S.-T. Chen, S. Thomas, K. J. Gaffney, S. G. Louie, N. A. Petasis and A. H. Schönthal, *Leukemia Research*, 2010, **34**, 250-253.
41. J. J. Virrey, Z. Liu, H.-Y. Cho, A. Kardosh, E. B. Golden, S. G. Louie, K. J. Gaffney, N. A. Petasis, A. H. Schönthal, T. C. Chen and F. M. Hofman, *Molecular Cancer Therapeutics*, 2010, **9**, 631-641.
42. A. Ferrario, S. Lim, F. Xu, M. Luna, K. J. Gaffney, N. A. Petasis, A. H. Schönthal and C. J. Gomer, *Cancer Letters*, 2011, **304**, 33-40.
43. A. H. Schönthal, T. C. Chen, F. M. Hofman, S. G. Louie and N. A. Petasis, *Expert Opinion on Investigational Drugs*, 2008, **17**, 197-208.
44. A. H. Schönthal, T. C. Chen, F. M. Hofman, S. G. Louie and N. A. Petasis, *Current Pharmaceutical Design*, 2011, **17**, 2428-2438.
45. D. N. Sarma, M. L. Barrett, M. L. Chavez, T. L. Dog, P. Gardiner, G. I. Giancaspro, R. Ko, G. B. Mahady, R. J. Marles and L. S. Pellicore, *Drug Safety*, 2008, **31**, 469-484.
46. N. P. Gullett, A. R. M. Ruhul Amin, S. Bayraktar, J. M. Pezzuto, D. M. Shin, F. R. Khuri, B. B. Aggarwal, Y.-J. Surh and O. Kucuk, *Seminars in Oncology*, 2010, **37**, 258-281.
47. S. N. Saldanha, R. Kala and T. O. Tollefsbol, *Experimental Cell Research*, 2014, **324**, 40-53.
48. M. Z. Fang, Y. Wang, N. Ai, Z. Hou, Y. Sun, H. Lu, W. Welsh and C. S. Yang, *Cancer Research*, 2003, **63**, 7563-7570.
49. N. T. Zaveri, *Life Sciences*, 2006, **78**, 2073-2080.
50. R. L. Thangapazham, A. K. Singh, A. Sharma, J. Warren, J. P. Gaddipati and R. K. Maheshwari, *Cancer Letters*, 2007, **245**, 232-241.
51. N. Khan and H. Mukhtar, *Cancer Letters*, 2008, **269**, 269-280.
52. X. Han, T. Shen and H. Lou, *International Journal of Molecular Sciences*, 2007, **8**, 950-988.
53. M. González-Vallinas, M. González-Castejón, A. Rodríguez-Casado and A. Ramírez de Molina, *Nutrition Reviews*, 2013, n/a-n/a.
54. I. Andújar, M. C. Recio, R. M. Giner and J. L. Rios, *Oxidative Medicine and Cellular Longevity*, 2012, **2012**, 23.
55. M. A. Martin, L. Goya and S. Ramos, *Food and Chemical Toxicology*, 2013, **56**, 336-351.
56. G. G. Mackenzie, J. M. Delfino, C. L. Keen, C. G. Fraga and P. I. Oteiza, *Biochemical Pharmacology*, 2009, **78**, 1252-1262.
57. S. Nam, D. M. Smith and Q. P. Dou, *J. Biol. Chem.*, 2001, **276**, 13322-13330.
58. A. Kazi, Z. Wang, N. Kumar, S. C. Falsetti, T. H. Chan and Q. P. Dou, *Anticancer Research*, 2004, **24**, 943-954.
59. K. R. Landis-Piowar, C. Huo, D. Chen, V. Milacic, G. Shi, T. H. Chan and Q. P. Dou, *Cancer Research*, 2007, **67**, 4303-4310.
60. Q. Dou, K. Landis-Piowar, D. Chen, C. Huo, S. Wan and T. Chan, *Inflammopharmacology*, 2008, **16**, 208-212.
61. Q. P. Dou, *Nutrition and Cancer*, 2009, **61**, 827-835.
62. D. Chen, S. B. Wan, H. Yang, J. Yuan, T. H. Chan and Q. P. Dou, *Advances in Clinical Chemistry*, 2011, **53**, 155-177.
63. S. Pamu, D. Chen, F. Morin, C. Huo, Q. Cui, Q. P. Dou and T. H. Chan, *MedChemComm*, 2012, **3**, 229-232.
64. M. Shen, T. H. Chan and Q. P. Dou, *Anticancer Agents Med. Chem.*, 2012, **12**, 891-901.
65. J. Kanwar, M. Taskeen, m. Mohammad, C. Huo, T. H. Chan and Q. P. Dou, *Frontiers in Bioscience*, 2012, **4**, 111-131.
66. Y. Fernández, T. P. Miller, C. Denoyelle, J. A. Esteban, W.-H. Tang, A. L. Bengston and M. S. Soengas, *J. Biol. Chem.*, 2006, **281**, 1107-1118.
67. F.-T. Liu, S. G. Agrawal, Z. Movasaghi, P. B. Wyatt, I. U. Rehman, J. G. Gribben, A. C. Newland and L. Jia, *Blood*, 2008, **112**, 3835-3846.
68. G. Perrone, T. Hideshima, H. Ikeda, Y. Okawa, E. Calabrese, G. Gorgun, L. Santo, D. Cirstea, N. Raju, D. Chauhan, M. Baccarani, M. Cavo and K. C. Anderson, *Leukemia*, 2009, **23**, 1679-1686.
69. T. Y. Kim, J. Park, B. Oh, H. J. Min, T.-S. Jeong, J. H. Lee, C. Suh, J.-W. Cheong, H. J. Kim, S.-S. Yoon, S. B. Park and D. S. Lee, *British Journal of Haematology*, 2009, **146**, 270-281.
70. B. Bannerman, L. Xu, M. Jones, C. Tsu, J. Yu, P. Hales, J. Monbaliu, P. Fleming, L. Dick, M. Manfredi, C. Claiborne, J. Bolen, E. Kupperman and A. Berger, *Cancer Chemotherapy and Pharmacology*, 2011, **68**, 1145-1154.
71. Q. Wang, J. Li, J. Gu, B. Huang, Y. Zhao, D. Zheng, Y. Ding and L. Zeng, *Acta Biochimica et Biophysica Sinica*, 2009, **41**, 1018-1026.
72. G. Springsteen and B. Wang, *Tetrahedron*, 2002, **58**, 5291-5300.
73. J. Yan, G. Springsteen, S. Deeter and B. Wang, *Tetrahedron*, 2004, **60**, 11205-11209.
74. J. Su, F. Chen, V. L. Cryns and P. B. Messersmith, *J. Am. Chem. Soc.*, 2011, **133**, 11850-11853.
75. M. A. Martínez-Aguirre, R. Villamil-Ramos, J. A. Guerrero-Alvarez and A. K. Yatsimirsky, *J. Org. Chem.*, 2013, **78**, 4674-4684.
76. J. D. Ashley, J. F. Stefanick, V. A. Schroeder, M. A. Suckow, T. Kiziltepe and B. Bilgicir, *J. Med. Chem.*, 2014, **57**, 5282-5292.
77. H. Chen, S. Viel, F. Ziarelli and L. Peng, *Chem. Soc. Rev.*, 2013, **42**, 7971-7982.
78. C. Dalvit, *Progress in Nuclear Magnetic Resonance Spectroscopy*, 2007, **51**, 243-271.
79. C. Dalvit, P. E. Fagerness, D. T. A. Hadden, R. W. Sarver and B. J. Stockman, *J. Am. Chem. Soc.*, 2003, **125**, 7696-7703.
80. A. Vulpetti, U. Hommel, G. Landrum, R. Lewis and C. Dalvit, *J. Am. Chem. Soc.*, 2009, **131**, 12949-12959.
81. M. Keita, J. Kaffy, C. Troufflard, E. Morvan, B. Crousse and S. Ongeri, *Org. Biomol. Chem.*, 2014, **12**, 4576-4581.
82. N. Jayatilaka, A. Han, K. J. Gaffney, R. Dey, J. A. Jarusiewicz, K. Noridomi, M. A. Philips, X. Lei, J. He, J. Ye, T. Gao, N. A. Petasis and L. Chen, *Nucleic Acids Research*, 2012, **40**, 5378-5388.
83. M. Groll, C. R. Berkens, H. L. Ploegh and H. Ovaa, *Structure*, 2006, **14**, 451-456.
84. N. Ni, G. Choudhary, M. Li and B. Wang, *Bioorganic & Medicinal Chemistry Letters*, 2008, **18**, 1567-1572.
85. Lee, S. J.; Gray, K. C.; Paek, J. S.; Burke, M. D. *J. Am. Chem. Soc.* 2007, **130**, 466-468.